

Probing Quantum Anomalous Hall States in Twisted Bilayer WSe₂ via Attractive Polaron Spectroscopy

Beini Gao,¹ Mahdi Ghafariasl,^{1,*} Mahmoud Jalali Mehrabad,^{1,*} Tsung-Sheng Huang,^{1,*} Lifu Zhang,¹ Deric Session,¹ Pranshoo Upadhyay,¹ Rundong Ma,² Ghadah Alshalan,¹ Daniel Suarez,¹ Supratik Sarkar,¹ Suji Park,³ Houk Jang,³ Kenji Watanabe,⁴ Takashi Taniguchi,⁴ Ming Xie,⁵ You Zhou,^{6,†} and Mohammad Hafezi^{1,‡}

¹*Joint Quantum Institute (JQI), University of Maryland, College Park, MD 20742, USA*

²*Electrical Engineering Department, University of Maryland, College Park, MD 20742, USA*

³*Center for Functional Nanomaterials, Brookhaven National Laboratory, Upton, NY 11973, USA.*

⁴*Research Center for Electronic and Optical Materials,*

National Institute for Materials Science, 1-1 Namiki, Tsukuba 305-0044, Japan.

⁵*Condensed Matter Theory Center, University of Maryland, College Park, MD, USA*

⁶*Department of Materials Science and Engineering, University of Maryland, College Park, MD 20742, USA*

(Dated: March 12, 2026)

Moiré superlattices in semiconductors exhibit a rich variety of interaction-induced topological states, including quantum anomalous Hall (QAH) effects [1–8]. A recent study hinted that twisted WSe₂ homobilayer (tWSe₂) could host a QAH state but lacked direct evidence of ferromagnetism, a key hallmark of this phase [9]. Here, we report the first direct evidence of QAH states in tWSe₂ with spontaneous ferromagnetism. Specifically, we employ polarization-resolved attractive polaron spectroscopy on a dual-gated, 2° tWSe₂ and observe direct signatures of spontaneous time-reversal symmetry breaking at hole filling $\nu = 1$. Together with a Chern number (C) measurement via Streda formula analysis, we identify this magnetized state as a topological state, characterized by $C = 1$. Furthermore, we demonstrate that these topological and magnetic properties are tunable via a finite displacement field, between a QAH ferromagnetic state and an antiferromagnetic state. Our findings position tWSe₂ as a highly versatile, stable, and optically addressable platform for investigating topological order and strong correlations in two-dimensional landscapes.

I. Introduction

Twisted transition metal dichalcogenide (TMD) bilayers have emerged as a highly tunable platform for investigating correlated electronic phases in two dimensions. In these systems, the presence of periodic moiré potentials — arising from lattice mismatch — produces strong interaction and non-trivial topology, resulting in a wide array of exotic many-body states. These include superconductivity [10, 11], ferroelectric order [12], Mott insulators [13–16], generalized Wigner crystals [13, 17, 18], and a growing set of topological phases, such as integer and fractional quantum spin Hall [19] and quantum anomalous Hall (QAH) states [1–8].

QAH phases are especially appealing as they exhibit topological properties even in the absence of an external magnetic field. Examples include integer and fractional QAH states in MoTe₂ [1–8], and integer QAH in twisted MoTe₂–WSe₂ heterobilayers [20]. Despite these advances, tWSe₂ remains largely underexplored even though it offers practical advantages, including enhanced air stability and visible-frequency optical transitions — features that make it an excellent platform for scalable device engineering and optical interrogation. Recent breakthrough experiments in tWSe₂ have demonstrated QAH effect at 1.2° twist angle [9], as well as superconductivity at 3.6° and 5° angles [10, 11]. However, ferromagnetism in the QAH states has yet to be unambiguously observed. The precise twist angular dependence of these emer-

gent states and their potential interplay has become a topic of significant interest.

Specifically, the magnetic and topological nature of correlated states in this system remains largely uncharted. For instance, clear signatures of spontaneous time-reversal symmetry breaking at integer fillings, and probe of the phase diagram in tWSe₂ have yet to be observed.

Here, we report the first optical detection of ferromagnetic and the quantum anomalous Hall state in tWSe₂, using attractive polaron (AP) spectroscopy [21]. Polarization-resolved reflection near the AP resonance reveals clear signatures of spontaneous magnetization at hole filling $\nu = 1$. Using the Streda formula, we identify this state as a Chern insulator with a Chern number $C = 1$, intriguingly opposite in sign to that reported in an earlier study in 1.23° tWSe₂ [9]. Our optical measurement establishes the presence of topological states on a macroscopic level, which is inaccessible via local scanning probes [9]. Furthermore, we demonstrate electric field control of a QAH ferromagnetic phase to an antiferromagnetic state in such a system.

II. Attractive Polaron Spectroscopy

Our sample is 2° twisted WSe₂ with a hexagonal structure whose superlattice periodicity is approximately 9.4 nm (see Supplemental Information Fig. 2 for calibration of twisting angle). The two sublattices in a moiré unit cell are denoted by MX and XM, respectively, as shown in Fig. 1a (see Supplemental Information Fig. 1 for the calculated electronic structure). We employ a dual-gate geometry to enable independent control of both the hole filling factor, ν , and the perpendic-

* These authors contributed equally to this work

† Corresponding author: youzhou@umd.edu

‡ Corresponding author: hafezi@umd.edu

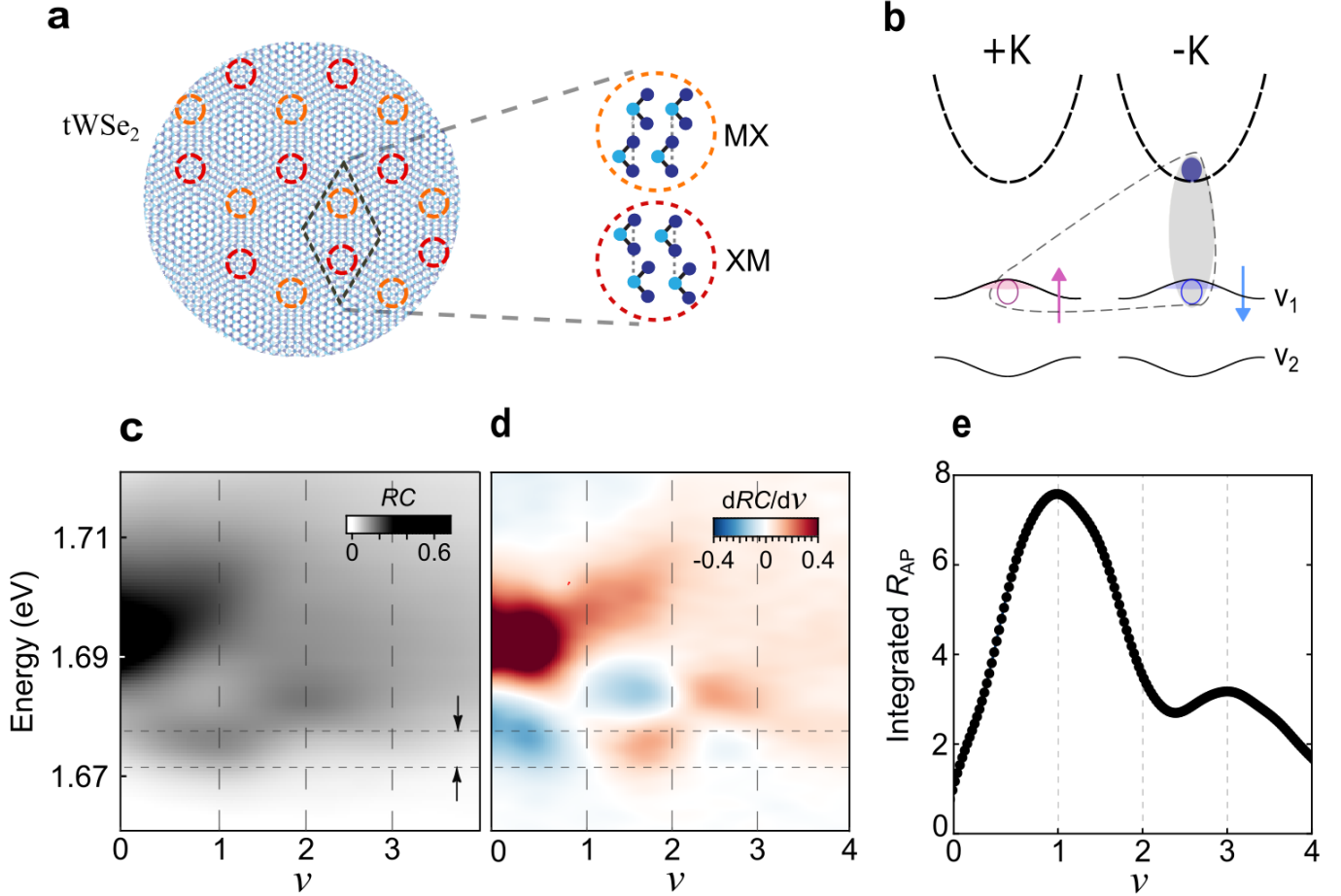
Fig.1: Attractive Polaron sensing of the incompressible states

FIG. 1. **a**, Illustration of the moiré pattern in a R-stacked twisted WSe₂ homobilayer. Orange and red circles denote the high-symmetry atomic registries MX and XM, respectively (see inset). **b**, Schematic of an attractive polaron (AP) formed by an exciton in one valley (here at $-K$) and a hole in the opposite valley ($+K$). The exciton consists of an electron in the lowest conduction moiré band (dashed) and a hole in the topmost valence moiré band (V_1). A second valence moiré band, V_2 , is separated from V_1 . **c**, Reflection contrast (RC) spectrum, defined as $\frac{R-R_0}{R_0}$, at temperature 4K. The hole-filling fraction ν is tuned by gates (see Methods for calibration). The horizontal dashed lines (and arrows) indicate the integrated energy range of the attractive polaron. **d**, Derivative of RC with respect to ν . **e**, Doping dependence of the integrated AP intensity (R_{AP}).

ular displacement field (D). Tuning D controls the interlayer potential difference in tWSe₂.

The attractive polaron in our system is a composite excitation between an exciton in one valley and a hole in the opposite valley, as shown schematically in Fig. 1b. Therefore, the polarization-resolved optical response at AP resonance reveals the hole occupancy in the opposite valley [21].

To identify and characterize the AP resonance, we measure the reflection contrast (RC) spectrum as a function of ν , which exhibits several resonances (Fig. 1c). Near the charge-neutral regime, we identify tWSe₂ intralayer excitons at 1.694 eV. As the system is hole-doped, we observe a continuously blue-shifting resonance of the repulsive polaron, and a red-shifting resonance (upon doping until $\nu = 1$) as the AP. We note that oscillator strength is transferred to a higher energy intrinsic species near $\nu = 2$. By analyzing the doping-dependent

derivative of RC , we identify two sign reversals at $\nu = 1$ and $\nu = 3$ (Fig. 1d), marking the peak of the oscillator strength of the AP. By integrating the AP intensity (within the horizontal dashed lines indicated in Fig. 1c), we observe that its oscillator strength increases monotonically with ν up to $\nu = 1$, then decreases between $\nu = 1$ and $\nu = 2$, as shown in Fig. 1e indicating a Hubbard picture where the AP oscillator strength scales with the number of singly occupied states in the valence moiré bands [23–26] (see Supplemental Information Fig. 1). The same trend repeats between $\nu = 2$ and $\nu = 4$.

To qualitatively understand the observed characteristics of AP, we use the fact that its oscillator strength scale with the number of singly occupied states in the valence moiré bands [21]. In other words, any creation of vacant and doubly occupied states transfers the AP oscillator strength to other species outside of the AP's integrated frequency range. Here,

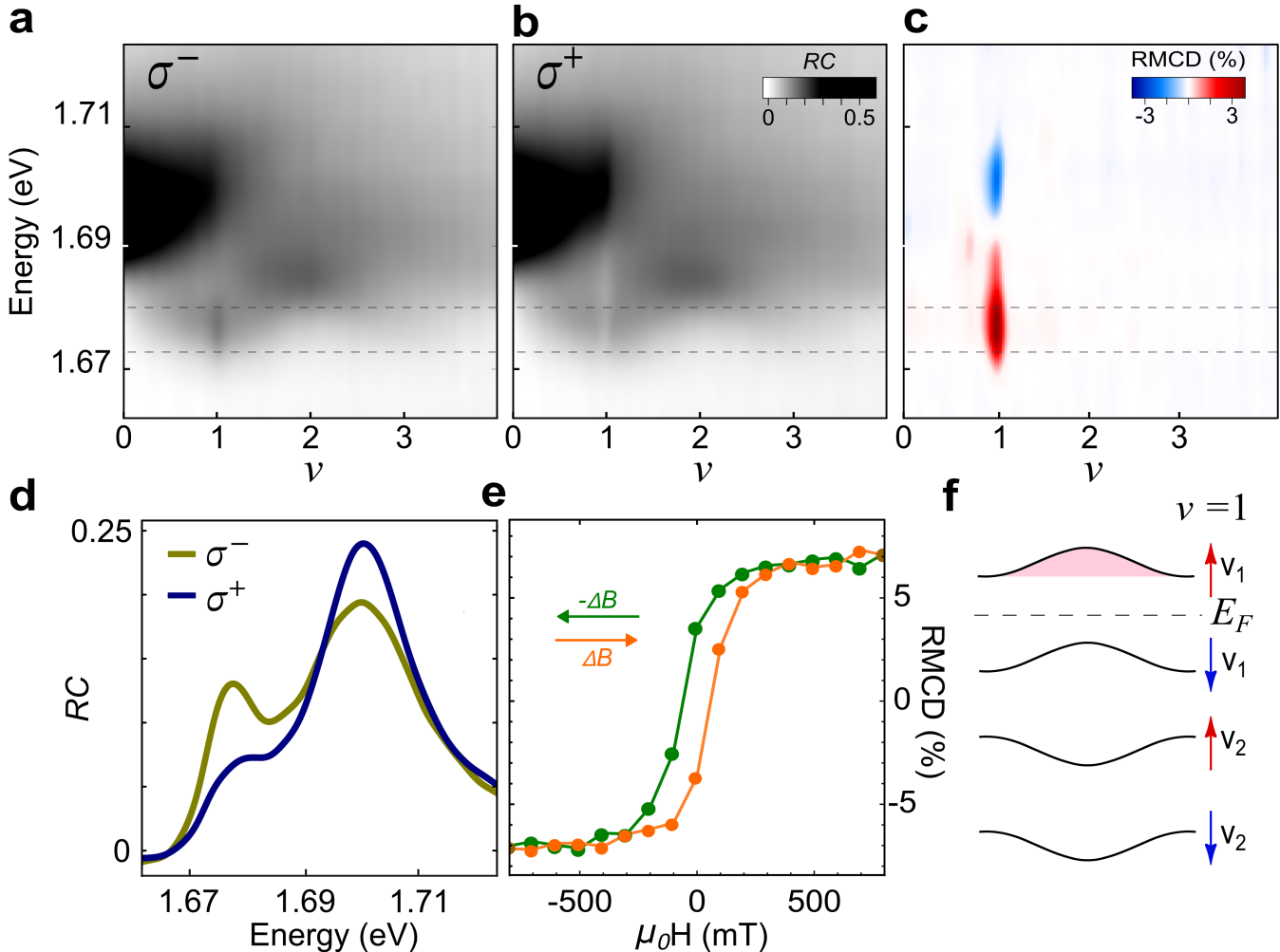
Fig.2: Spontaneous magnetization at $\nu = 1$.

FIG. 2. RC as a function of energy and hole filling fraction ν under **a**, σ^- and **b**, σ^+ excitation, respectively. **c**, Spectrally resolved reflection magnetic circular dichroism (RMCD) at various ν . **d**, Polarization-resolved reflection spectrum at $\nu = 1$. **e**, Magnetic hysteresis loop measured at $\nu = 1$; green and orange indicate the scan directions with respect to the magnetic field ($\pm\Delta B$). **f**, Schematic of the *many-body* bands at $\nu = 1$, incorporating electrostatic interaction at the mean-field level [22]. ν_1 and ν_2 denote the first and the second moiré valence bands, respectively. This diagram is specific to $\nu = 1$ and does not represent the band structure at other fillings.

All the data were taken at a lattice temperature $T_{\text{lattice}} = 66$ mK.

we note that at $\nu = 1$, there is a single hole per moiré unit cell, and therefore, gives the maximum number of singly occupied states for the topmost moiré valence band ν_1 (Fig. 1b). The observed repeating oscillator strength trend for $\nu > 2$ in Fig. 1e follows a similar explanation for the second moiré band ν_2 . In addition, independent measurements using a MoSe₂ sensing layer (see Supplemental Information Fig. 16) reveals suppressed compressibility at $\nu = 1$, corroborating that the AP maximum corresponds to a correlated insulating state.

III. Spontaneous magnetization at $\nu = 1$

To optically detect spontaneous magnetization of the sys-

tem, we measure polarization-resolved RC under zero magnetic field (Fig. 2a-b) and construct the reflection magnetic circular dichroism (RMCD) as a function of ν at 66 mK, as shown in Fig. 2c. Since the RC from σ_- and σ_+ excitations selectively probe the occupation of doped charges in the $+K$ and $-K$ valleys, respectively, any valley and spin imbalance will lead to a different optical response in the two polarizations. Remarkably, we observe that the RC exhibits a pronounced peak for σ_- excitation at $\nu = 1$, while a dip is observed for σ_+ within the AP energy range, a direct indication of spontaneous time-reversal symmetry breaking. To be more quantitative, the RMCD measurement in Fig. 2c captures the out-of-plane magnetization of the doped charges. The magnetization peaks at $\nu = 1$ (see Fig. 2d for RC spectra), while it

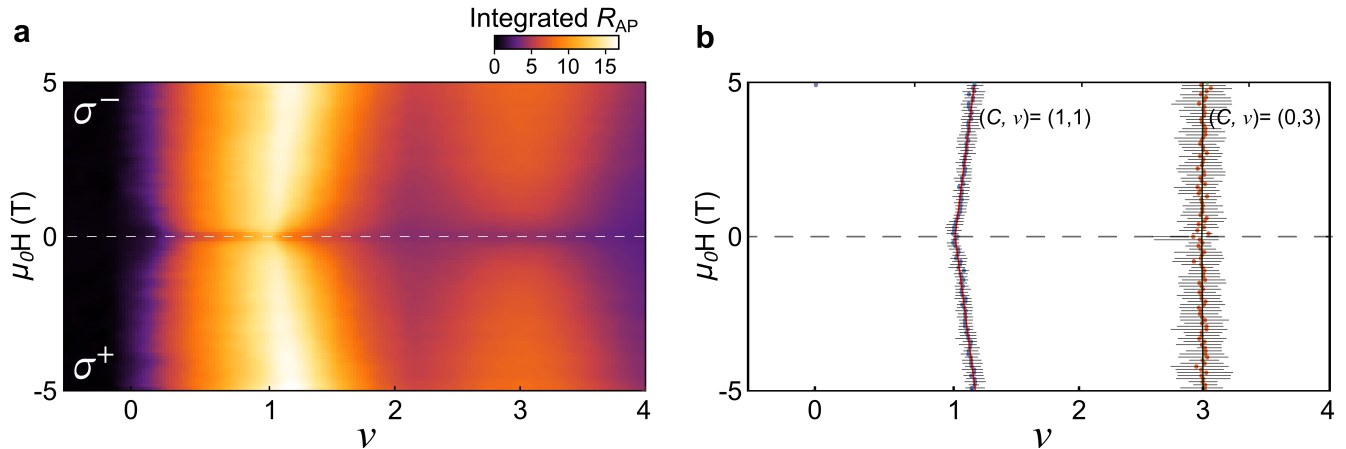
Fig. 3: Identifying the QAH states with the Streda formula

FIG. 3. **a**, Integrated AP intensity as a function of magnetic field $\mu_0 H$ and hole filling ν . **b**, Extracted maxima of the integrated AP intensity at each $\mu_0 H$ near $\nu \simeq 1, 3$, indicated by blue, and orange points, respectively. Error bars represent 3% deviation from the centroid for $\nu = 1$ and 5% deviation for $\nu = 3$ (see Methods). Red and dark green lines near $\nu = 1$ and $\nu = 3$, from which the slope indicates Chern number $C = 1$ for $\nu = 1$, and $C = 0$ for $\nu = 3$.

remains negligible at other fillings.

Crucially, in addition to spontaneous RMCD under a zero field, we observe a magnetic hysteresis loop at $\nu = 1$, which indicates the presence of ferromagnetism (FM), with a coercive magnetic field of approximately 50 mT, as shown in Fig. 2e. The observed emergent magnetism can be understood in the mean-field approximation, where electron-electron interactions generate an effective exchange splitting between the two valleys, yielding FM around $\nu = 1$ as only one valley is occupied, as schematically illustrated in Fig. 2f. The hysteresis disappears at a higher temperature of around 1.2 K, see Supplemental Information Fig. 3. Notably, our observation of FM at $\nu = 1$ in tWSe₂ is similar to the general trend seen in MoTe₂; however, here we report the absence of FM at $\nu = 3$, in contrast to MoTe₂.

IV. Identifying the quantum anomalous Hall state with Streda formula

To directly determine the topological properties of our system, we measure the magnetic field- and doping-dependence of the optical spectra and extract the topological invariant from the Streda formula [1, 27–29]. Specifically, we track the frequency-integrated oscillator strength, as a function of magnetic field $\mu_0 H$ and gate voltage (see Supplemental Information Fig. 4-6 for details). In particular, the AP spectroscopy performed at $\nu > 0$ allows us to track the density shift of correlated states as a function of the magnetic field $\mu_0 H$, as shown in Fig. 3a. The local maxima therein for each $\mu_0 H$ is extracted and shown in Fig. 3b, and the slope of each line indicates the Chern number (C) of the corresponding state.

The polaron peak at $\nu = 1$ marks a correlated insulating state whose density shifts linearly as a function of the magnetic field, with a slope that matches $C = 1$, according to the Streda formula. The sign of the slope indicates that the total

magnetization of the $\nu = 1$ ground state has the same sign as the Chern number. Interestingly, this measured Chern number has the opposite sign compared to recent reports in tWSe₂ [9] with a smaller twist angle of 1.23° , potentially due to the twist angle difference and lattice relaxation [30, 31]. Together with the emergence of FM at this filling, we attribute this state to an integer QAH phase. Upon reversal of the magnetic field, the magnetization reverses, which also leads to a reversal of the Chern number to $C = -1$, manifesting a valley contrasting Chern number for the many-body ground state. Compared to twisted MoTe₂, the lack of an experimentally observed QAH phase in earlier experiments employing twisted WSe₂ [32] may be attributed to its significantly lower ferromagnetic transition temperature, $T_C < 1.2$ K, in contrast to $T_C \approx 10$ K in MoTe₂. We also note that at twist angles smaller than the current studies, such as $\theta \leq 1.5^\circ$, tWSe₂ can suffer a stronger lattice relaxation effect compared to tMoTe₂. This can lead to high twist angle disorder, as was the case in earlier local probe measurement [9].

In contrast to the QAH state at $\nu = 1$, the feature at $\nu = 3$ shows vanishing Streda slope and therefore is compatible with a zero Chern number $C = 0$. This may suggest a topologically trivial correlated phase, such as an intervalley coherent or antiferromagnetic state, which has not been observed previously reported in higher moiré bands of this system [8, 19, 33], or potentially a non-Abelian spin Hall insulator, as theoretically predicted [34]. Further investigation will be required to clarify the character of the $\nu = 3$ state.

V. Displacement field tuning: from QAH FM to AFM

With QAH physics at $\nu = 1$ established under a zero displacement field, we further investigate the robustness and tunability of this Chern insulating state with a finite displacement

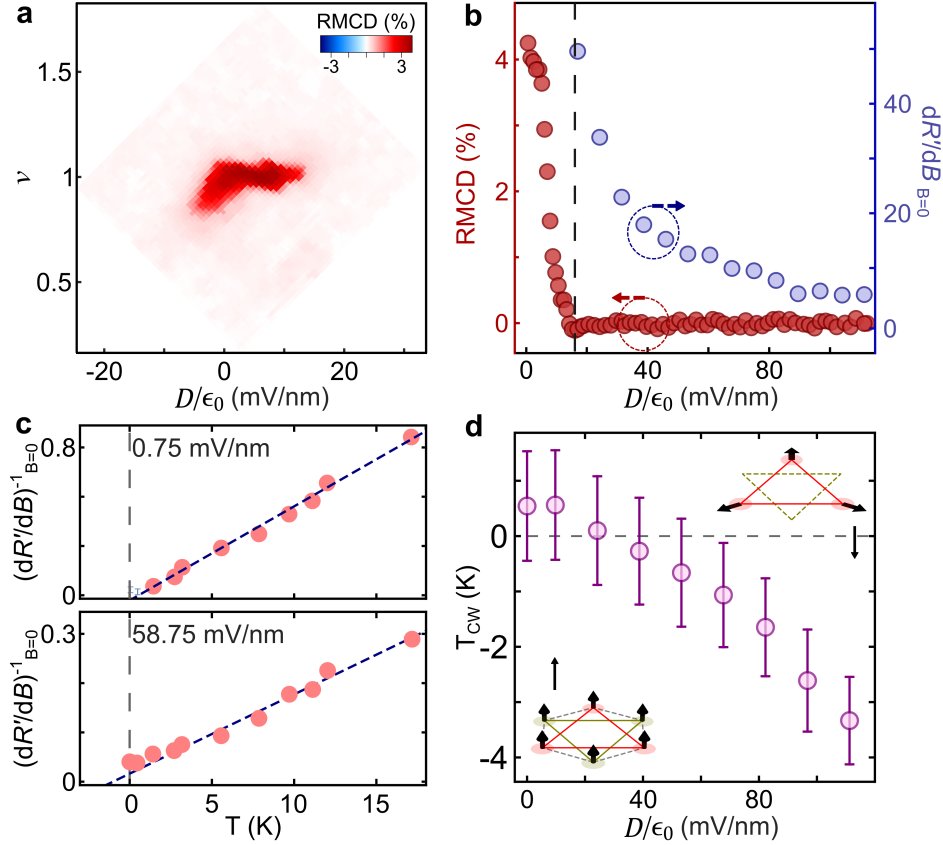
Fig. 4: Displacement field tuning: from QAH FM to AFM.

FIG. 4. **a**, RMCD as a function of the displacement field D and hole filling fraction ν at magnetic field $B = 0$ and temperature $T_{\text{lattice}} = 66$ mK. **b**, (Red, left y-axis) Reflection magnetic circular dichroism (RMCD) as a function of the displacement field $\frac{D}{\epsilon_0}$ at $B = 0$. (Blue, right y-axis) derivative of RMCD with respect to magnetic field B at $B = 0$ measured as a function of $\frac{D}{\epsilon_0}$. **c**, Magnetic susceptibility as a function of temperature for two displacement field values. The dashed line is the Curie-Weiss fit. All the small displacement field fittings are done with data points above the Curie temperature of ~ 1.2 K, see Supplemental Information Fig. 3, Fig. 9. **d**, Curie-Weiss temperature T_{CW} as a function of $\frac{D}{\epsilon_0}$. Linear fitting error bars are also shown. The inset schematics indicate the (bottom) QAH FM phase and the (top) AFM phase, respectively.

field D/ϵ_0 . First, in Fig. 4a, we present the RMCD diagram with respect to ν and D/ϵ_0 at zero magnetic field and lattice temperature of 66 mK. We observe a prominent RMCD response at around $\nu = 1$, where the RMCD signal persists up to ~ 18 mV/nm. This region of a prominent RMCD response establishes the ferromagnetic regime in the overall phase diagram of $tWSe_2$. At a slightly elevated magnetic field of 0.1 T, the ferromagnetic phase becomes further stabilized across a broader regime (Supplemental Information Fig. 8). Notably, ferromagnetic order is stabilized near the van Hove singularity, suggesting enhanced interaction strength due to the high density of states (Supplemental Information Fig. 8) [10, 11, 32].

Focusing on the displacement-field-dependence of the RMCD at $\nu = 1$, we observe that the magnetization of the system quenches above a critical displacement field of 18 mV/nm, as indicated by the dashed line in Fig. 4b. Meanwhile, near this critical displacement field, we also observe a divergent magnetic susceptibility ($\chi = dR'/dB$, where R' stands for RMCD), consistent with a field-controlled magnetic

phase transition (Fig. 4b, see Supplemental Information Fig. 7 for spectrally resolved data).

To understand the origin of this magnetic phase transition, we measure the magnetic susceptibility of the sample by performing temperature-dependent RMCD measurements and extract the Curie-Weiss temperature T_{CW} (see Supplemental Information Fig. 9 for details). Intriguingly, we observe a clear sign-change of the Curie-Weiss temperature T_{CW} , as shown in Fig. 4c, from positive to negative with increasing D . This indicates a transition from FM to antiferromagnetic (AFM) order [24, 35] in our system, due to a change in the lattice geometry as shown schematically in the inset of Fig. 4d. A finite D introduces a layer-dependent potential that polarizes the moiré valence band toward one physical layer, thereby suppressing interlayer hybridization and redistributing the Berry curvature. Our numerical calculations (Supplemental Information Fig. 10) confirm that increasing interlayer bias progressively shifts the Berry curvature weight from the K region toward K' , driving the transition from

$C = 1$ to $C = 0$. Together, these findings reveal a field-tunable magnetic phase transition linked to the underlying topological properties of the correlated moiré system.

Conclusion

In summary, we have reported the first optical detection of the QAH states in a tWSe₂ system and demonstrated displacement-field tunability of the underlying magnetic order, showcasing transitions between quantum anomalous Hall ferromagnetic and antiferromagnetic phases. These results highlight tWSe₂ as a uniquely versatile platform, combining visible-frequency optical access with air stability and fabrication simplicity—features that open new directions for probing correlated and topological quantum phases in moiré systems.

Looking ahead, several exciting research avenues can be built upon our findings. One promising direction is the exploration of fractional Chern insulators [36], which have recently been observed in tMoTe₂ [1–4, 37–39], and whose realization in tWSe₂ would open access to new correlated topological phases. Furthermore, similar to the recently demonstrated coexistence of QAH and superconductivity in tMoTe₂ [40], we anticipate intriguing interplay between topological states and superconductivity in tWSe₂ [10, 11]. Moreover, the presence of different Chern numbers in higher moiré bands compared to MoTe₂ may lead to the realization of other correlated states [30]. More intriguing is the realization of recently predicted topological excitons [41], accessible in a modified device architecture designed to host long-lived interlayer excitons. The coexistence of strong exciton-exciton interactions [15, 16, 42, 43] and tunable excitonic band topology [41] offers a compelling pathway toward the realization of bosonic fractional Chern insulators [44–46]. Such long-sought phase are bosonic analogue of fermionic fractional Chern insulators [47–51], which has remained unobserved in any system to date. More generally, this system could be considered as a promising candidate for optical probe and manipulation of strongly-correlated electron-photon systems [52, 53]. Specifically, interesting prospects are optical detection and manipulation of topological states [54, 55].

Methods

Device fabrication

The device was made by “tear-and-stack” technique using the standard polymer-based dry transfer method. With picking up the top gate graphite, top gate hBN, tWSe₂, bilayer hBN spacer, half overlapped MoSe₂ monolayer in sequence and dropped down onto a pre-prepared hBN-Graphite bottom gate on a 285 nm SiO₂/Si substrate. Followed by electron beam lithography and metal deposition for the gate and contacts (5 nm Cr, 70 nm Au). All the monolayers are identified via optical contrast. The top (~ 17.8 nm) and bottom (~ 24.6 nm) dielectric hBN thickness are confirmed by atomic force microscopy.

Optical measurements

Optical measurements were performed using confocal microscopy in an optically accessible dilution fridge (BlueFors) with vertical magnetic fields up to 9T and temperatures down to a lattice temperature of 60 mK [56]. A halogen lamp was used as the light source. The input light was spectrally filtered to 650 to 900 nm range. A low-temperature microscope objective was used to focus the light onto the sample. The light intensity on the sample was kept around $0.14 \text{ nW}/\mu\text{m}^2$ to minimize its effects on the electronic states. The reflected light was collected by the same objective and analyzed by a spectrometer equipped with a charge coupled device array to obtain spectrum. The RC spectrum is defined as $(R - R_0)/R$, where R_0 the reference spectrum was taken for the sample at a high doping density with quenched excitonic resonances. For all the zero magnetic field data presented in Fig. 2 and 4, we polarize the system with a positive vertical magnetic field and then ramp back to perform the zero magnetic field measurement. The RMCD was used to study the magnetic properties of the samples. A combination of a linear polarizer and a quarter-wave plate was used to generate circularly polarized light (σ_- and σ_+) on the sample. The RMCD spectrum is defined as $\frac{\sigma_- - \sigma_+}{\sigma_- + \sigma_+}$.

For the AP spectroscopy, we integrate the reflectance over a range of wavelengths (738-741.2 nm, or equivalently, 1.673 - 1.680 eV) that focuses on the attractive polaron resonance of tWSe₂. The same wavelength range was used to obtain the average of the absolute value of RMCD. The magnetic susceptibility was evaluated from the slope of MCD at zero magnetic field.

For the streda formula data presented in Fig. 3, we use RC under σ^- excitation for the positive magnetic field detection, and σ^+ excitation for the negative magnetic field detection.

Twist Angle Calibration

We calibrate the twist angle of the tWSe₂ presented in the main text using the quantum oscillations observed optically under an out-of-plane magnetic field of 8.8T. In Supplemental Information Fig. 2, we present the doping dependent RC response of a monolayer tWSe₂ under σ_+ excitation. The oscillation signal formed as a result of the formation of the Landau levels (LLs). The LL period is determined to be 0.244 V for the single gate response, from which we deduce a hole density change of $1.75 \times 10^{12} \text{ cm}^{-2}$ per volt for data presented in the main text. Combining with the moiré period ΔV_M extracted from the doping dependent RC data, we obtain a moiré density n_M of $1.31 \times 10^{12} \text{ cm}^{-2}$. The twist angle calibration is further corroborated by the doping density calibration, as described in the next section.

Doping density calibration

A parallel-plate capacitor model is used to calculate the gate-induced carrier density n and displacement field D based on the applied gate voltages. The gate capacitances per area of the top and bottom gates, $C_{t/b} = \epsilon_{\text{hBN}} \epsilon_0 / d_{t/b}$, are determined by the hBN thickness $d_{t/b}$ and dielectric constant.

We use $\epsilon_{hBN} = 3.89$ here. The sample doping density n can be calculated as $n = (C_t V_t + C_b V_b)$, where V_t and V_b are the voltages applied to the top and bottom gates. The displacement field is defined as $D = (C_t V_t - C_b V_b)/2\epsilon_0 - D_{\text{offset}}$, where ϵ_0 is the vacuum permittivity and the subtracted value is the built-in offset.

Extraction and analysis of the Streda signal

To extract the Streda response, we first obtain polarization-resolved reflection-contrast (RC) spectra as a function of gate voltage and magnetic field. For each magnetic-field value, an energy window containing the attractive-polaron (AP) resonance is integrated to yield an intensity map $I_{\text{AP}}(\nu, \mu_0 H)$, where ν is the hole filling. The resulting $I_{\text{AP}}(\nu)$ curve exhibits local maxima at incompressible fillings. We identify this maximum from the derivative of I_{AP} with respect to ν and treat its position $\nu_{\text{max}}(B)$ as the quantity entering the Streda analysis.

The uncertainty in each extracted ν_{max} is estimated by computing the centroid of the AP peak at fixed magnetic field and defining an error range corresponding to a deviation of the integrated intensity from the centroid. For the sharp $\nu = 1$ feature we use a 3% deviation; for the broader $\nu = 3$ feature we use 5%.

The Streda slope $d\nu/dB$ is then obtained from a linear fit to $\nu_{\text{max}}(B)$ near the filling of interest. Using the Streda relation $C = \frac{h}{e} \frac{d\nu}{dB}$, we extract the corresponding Chern number.

To verify robustness, we repeat the analysis using several different integration windows for the AP resonance (widths of 3.05 meV, 5.71 meV, and 8.85 meV). All choices yield consistent slopes within the extracted uncertainties.

Acknowledgements: We thank Ataç İmamoğlu, Liang Fu, Sankar Das Sarma, Ajit Srivastava, Patrick Knüppel, Xiaowei Zhang for fruitful discussions.

Author Contributions: B.G., Y.Z., and M.H. conceived the project. B.G. performed the optical measurements and analyzed the data. M.X. did the theoretical calculation. M.X. and T.S.H. contributed to the theoretical understanding. L.Z. and B.G. fabricated the device. L.Z., M.G., D.S., P.U., G.A., R.M., M.J.M., and S.S. assisted with the experiment. S.J. and H.J. exfoliated the TMD flakes. T.T. and K.W. provided the bulk h-BN crystals. All authors contributed the writing of the manuscript. Y.Z. and M.H. supervised the work. All authors discussed the results and contributed to the manuscript.

Competing interests: The authors declare no competing interests.

Data availability: All of the data that support the findings of this study are reported in the main text and Supplementary Information. Source data are available from the corresponding authors on reasonable request.

-
- [1] J. Cai, E. Anderson, C. Wang, X. Zhang, X. Liu, W. Holtzmann, Y. Zhang, F. Fan, T. Taniguchi, K. Watanabe, *et al.*, Signatures of fractional quantum anomalous hall states in twisted mote2, *Nature* **622**, 63 (2023).
- [2] Y. Zeng, Z. Xia, K. Kang, J. Zhu, P. Knüppel, C. Vaswani, K. Watanabe, T. Taniguchi, K. F. Mak, and J. Shan, Thermodynamic evidence of fractional chern insulator in moiré mote2, *Nature* **622**, 69 (2023).
- [3] H. Park, J. Cai, E. Anderson, Y. Zhang, J. Zhu, X. Liu, C. Wang, W. Holtzmann, C. Hu, Z. Liu, *et al.*, Observation of fractionally quantized anomalous hall effect, *Nature* **622**, 74 (2023).
- [4] F. Xu, Z. Sun, T. Jia, C. Liu, C. Xu, C. Li, Y. Gu, K. Watanabe, T. Taniguchi, B. Tong, *et al.*, Observation of integer and fractional quantum anomalous hall effects in twisted bilayer mote 2, *Physical Review X* **13**, 031037 (2023).
- [5] Z. Ji, H. Park, M. E. Barber, C. Hu, K. Watanabe, T. Taniguchi, J.-H. Chu, X. Xu, and Z.-X. Shen, Local probe of bulk and edge states in a fractional chern insulator, *Nature* **635**, 578 (2024).
- [6] E. Redekop, C. Zhang, H. Park, J. Cai, E. Anderson, O. Sheekey, T. Arp, G. Babikyan, S. Salters, K. Watanabe, *et al.*, Direct magnetic imaging of fractional chern insulators in twisted mote2, *Nature* **635**, 584 (2024).
- [7] F. Xu, X. Chang, J. Xiao, Y. Zhang, F. Liu, Z. Sun, N. Mao, N. Peshchenko, J. Li, K. Watanabe, *et al.*, Interplay between topology and correlations in the second moiré band of twisted bilayer mote2, *Nature Physics* , 1 (2025).
- [8] H. Park, J. Cai, E. Anderson, X.-W. Zhang, X. Liu, W. Holtzmann, W. Li, C. Wang, C. Hu, Y. Zhao, *et al.*, Ferromagnetism and topology of the higher flat band in a fractional chern insulator, *Nature Physics* , 1 (2025).
- [9] B. A. Foutty, C. R. Kometter, T. Devakul, A. P. Reddy, K. Watanabe, T. Taniguchi, L. Fu, and B. E. Feldman, Mapping twist-tuned multiband topology in bilayer wse2, *Science* **384**, 343 (2024).
- [10] Y. Xia, Z. Han, K. Watanabe, T. Taniguchi, J. Shan, and K. F. Mak, Superconductivity in twisted bilayer wse2, *Nature* **637**, 833 (2025).
- [11] Y. Guo, J. Pack, J. Swann, L. Holtzman, M. Cothrine, K. Watanabe, T. Taniguchi, D. G. Mandrus, K. Barmak, J. Hone, *et al.*, Superconductivity in 5.0° twisted bilayer wse2, *Nature* **637**, 839 (2025).
- [12] A. Weston, E. G. Castanon, V. Enaldiev, F. Ferreira, S. Bhattacharjee, S. Xu, H. Corte-León, Z. Wu, N. Clark, A. Summerfield, *et al.*, Interfacial ferroelectricity in marginally twisted 2d semiconductors, *Nature nanotechnology* **17**, 390 (2022).
- [13] E. C. Regan, D. Wang, C. Jin, M. I. Bakti Utama, B. Gao, X. Wei, S. Zhao, W. Zhao, Z. Zhang, K. Yumigeta, M. Blei, J. D. Carlström, K. Watanabe, T. Taniguchi, S. Tongay, M. Crommie, A. Zettl, and F. Wang, Mott and generalized Wigner crystal states in WSe2/WS2 moiré superlattices, *Nature* 2020 579:7799 **579**, 359 (2020).
- [14] Y. Tang, L. Li, T. Li, Y. Xu, S. Liu, K. Barmak, K. Watanabe, T. Taniguchi, A. H. MacDonald, J. Shan, *et al.*, Simulation of hubbard model physics in wse2/ws2 moiré superlattices, *Nature* **579**, 353 (2020).
- [15] R. Xiong, J. H. Nie, S. L. Brantly, P. Hays, R. Sailus, K. Watanabe, *et al.*, Observation of a fractional quantum anomalous hall state in a twisted bilayer chern insulator, *Nature* **637**, 833 (2025).

- abe, T. Taniguchi, S. Tongay, and C. Jin, Correlated insulator of excitons in wse_2/wse_2 moiré superlattices, *Science* **380**, 860 (2023).
- [16] B. Gao, D. G. Suárez-Forero, S. Sarkar, T.-S. Huang, D. Session, M. J. Mehrabad, R. Ni, M. Xie, P. Upadhyay, J. Vannucci, *et al.*, Excitonic mott insulator in a bose-fermi-hubbard system of moiré wse_2/wse_2 heterobilayer, *Nature Communications* **15**, 2305 (2024).
- [17] Y. Xu, S. Liu, D. A. Rhodes, K. Watanabe, T. Taniguchi, J. Hone, V. Elser, K. F. Mak, and J. Shan, Correlated insulating states at fractional fillings of moiré superlattices, *Nature* **587**, 214 (2020).
- [18] Y. Zhou, J. Sung, E. Brutschea, I. Esterlis, Y. Wang, G. Scuri, R. J. Gelly, H. Heo, T. Taniguchi, K. Watanabe, *et al.*, Bilayer wigner crystals in a transition metal dichalcogenide heterostructure, *Nature* **595**, 48 (2021).
- [19] K. Kang, B. Shen, Y. Qiu, Y. Zeng, Z. Xia, K. Watanabe, T. Taniguchi, J. Shan, and K. F. Mak, Evidence of the fractional quantum spin hall effect in moiré wse_2 , *Nature* **628**, 522 (2024).
- [20] T. Li, S. Jiang, B. Shen, Y. Zhang, L. Li, Z. Tao, T. Devakul, K. Watanabe, T. Taniguchi, L. Fu, *et al.*, Quantum anomalous hall effect from intertwined moiré bands, *Nature* **600**, 641 (2021).
- [21] L. Ciorciaro, T. Smoleński, I. Morera, N. Kiper, S. Hiestand, M. Kroner, Y. Zhang, K. Watanabe, T. Taniguchi, E. Demler, *et al.*, Kinetic magnetism in triangular moiré materials, *Nature* **623**, 509 (2023).
- [22] F. Wu, T. Lovorn, E. Tutuc, I. Martin, and A. MacDonald, Topological insulators in twisted transition metal dichalcogenide homobilayers, *Physical review letters* **122**, 086402 (2019).
- [23] L. Wang, E.-M. Shih, A. Ghiotto, L. Xian, D. A. Rhodes, C. Tan, M. Claassen, D. M. Kennes, Y. Bai, B. Kim, *et al.*, Correlated electronic phases in twisted bilayer transition metal dichalcogenides, *Nature materials* **19**, 861 (2020).
- [24] H. Pan, F. Wu, and S. Das Sarma, Band topology, hubbard model, heisenberg model, and dzyaloshinskii-moriya interaction in twisted bilayer wse_2 , *Physical Review Research* **2**, 033087 (2020).
- [25] J. Zang, J. Wang, J. Cano, and A. J. Millis, Hartree-fock study of the moiré hubbard model for twisted bilayer transition metal dichalcogenides, *Physical Review B* **104**, 075150 (2021).
- [26] D. Muñoz-Segovia, V. Crépel, R. Queiroz, and A. J. Millis, Twist-angle evolution of the intervalley-coherent antiferromagnet in twisted wse_2 , *Physical Review B* **112**, 085111 (2025).
- [27] Y. Xie, A. T. Pierce, J. M. Park, D. E. Parker, E. Khalaf, P. Ledwith, Y. Cao, S. H. Lee, S. Chen, P. R. Forrester, *et al.*, Fractional chern insulators in magic-angle twisted bilayer graphene, *Nature* **600**, 439 (2021).
- [28] K. P. Nuckolls, M. Oh, D. Wong, B. Lian, K. Watanabe, T. Taniguchi, B. A. Bernevig, and A. Yazdani, Strongly correlated chern insulators in magic-angle twisted bilayer graphene, *Nature* **588**, 610 (2020).
- [29] E. M. Spanton, A. A. Zibrov, H. Zhou, T. Taniguchi, K. Watanabe, M. P. Zaletel, and A. F. Young, Observation of fractional chern insulators in a van der waals heterostructure, *Science* **360**, 62 (2018).
- [30] X.-W. Zhang, C. Wang, X. Liu, Y. Fan, T. Cao, and D. Xiao, Polarization-driven band topology evolution in twisted wse_2 and wse_2 , *Nature Communications* **15**, 4223 (2024).
- [31] T. Devakul, V. Crépel, Y. Zhang, and L. Fu, Magic in twisted transition metal dichalcogenide bilayers, *Nature communications* **12**, 6730 (2021).
- [32] P. Knüppel, J. Zhu, Y. Xia, Z. Xia, Z. Han, Y. Zeng, K. Watanabe, T. Taniguchi, J. Shan, and K. F. Mak, Correlated states controlled by a tunable van hove singularity in moiré wse_2 bilayers, *Nature Communications* **16**, 1959 (2025).
- [33] K. Kang, Y. Qiu, K. Watanabe, T. Taniguchi, J. Shan, and K. F. Mak, Double quantum spin hall phase in moiré wse_2 , *Nano Letters* **24**, 14901 (2024).
- [34] A. Abouelkomsan and L. Fu, Non-abelian spin hall insulator, *Physical Review Research* **7**, 023083 (2025).
- [35] E. Anderson, F.-R. Fan, J. Cai, W. Holtzmann, T. Taniguchi, K. Watanabe, D. Xiao, W. Yao, and X. Xu, Programming correlated magnetic states with gate-controlled moiré geometry, *Science* **381**, 325 (2023).
- [36] V. Crépel and L. Fu, Anomalous hall metal and fractional chern insulator in twisted transition metal dichalcogenides, *Physical Review B* **107**, L201109 (2023).
- [37] X. Chang, F. Liu, F. Xu, C. Xu, J. Xiao, Z. Sun, P. Jiao, Y. Zhang, S. Wang, B. Shen, R. He, K. Watanabe, T. Taniguchi, R. Zhong, J. Jia, Z. Shi, X. Liu, Y. Zhang, D. Qian, T. Li, and S. Jiang, Emergent charge-transfer ferromagnetism and fractional chern states in moiré wse_2 (2025), arXiv:2503.13213 [cond-mat.mes-hall].
- [38] Y. Wang, J. Choe, E. Anderson, W. Li, J. Ingham, E. A. Arsenault, Y. Li, X. Hu, T. Taniguchi, K. Watanabe, X. Roy, D. Basov, D. Xiao, R. Queiroz, J. C. Hone, X. Xu, and X. Y. Zhu, Hidden states and dynamics of fractional fillings in wse_2 moiré superlattices (2025), arXiv:2502.21153 [cond-mat.str-el].
- [39] E. Anderson, H. Park, K. Yang, J. Cai, T. Taniguchi, K. Watanabe, L. Fu, T. Cao, D. Xiao, and X. Xu, Magnetoelectric control of helical light emission in a moiré chern magnet (2025), arXiv:2503.02810 [cond-mat.mes-hall].
- [40] F. Xu, Z. Sun, J. Li, C. Zheng, C. Xu, J. Gao, T. Jia, K. Watanabe, T. Taniguchi, B. Tong, L. Lu, J. Jia, Z. Shi, S. Jiang, Y. Zhang, Y. Zhang, S. Lei, X. Liu, and T. Li, Signatures of unconventional superconductivity near reentrant and fractional quantum anomalous hall insulators (2025), arXiv:2504.06972 [cond-mat.mes-hall].
- [41] M. Xie, M. Hafezi, and S. Das Sarma, Long-lived topological flatband excitons in semiconductor moiré heterostructures: A bosonic kane-mele model platform, *Physical Review Letters* **133**, 136403 (2024).
- [42] H. Park, J. Zhu, X. Wang, Y. Wang, W. Holtzmann, T. Taniguchi, K. Watanabe, J. Yan, L. Fu, T. Cao, *et al.*, Dipole ladders with large hubbard interaction in a moiré exciton lattice, *Nature Physics* **19**, 1286 (2023).
- [43] Z. Lian, Y. Meng, L. Ma, I. Maity, L. Yan, Q. Wu, X. Huang, D. Chen, X. Chen, X. Chen, *et al.*, Valley-polarized excitonic mott insulator in wse_2/wse_2 moiré superlattice, *Nature Physics* **20**, 34 (2024).
- [44] M. Hafezi, A. S. Sørensen, E. Demler, and M. D. Lukin, Fractional quantum hall effect in optical lattices, *Physical Review A—Atomic, Molecular, and Optical Physics* **76**, 023613 (2007).
- [45] G. Möller and N. R. Cooper, Composite fermion theory for bosonic quantum hall states on lattices, *Physical Review Letters* **103**, 105303 (2009).
- [46] Y.-F. Wang, Z.-C. Gu, C.-D. Gong, and D. Sheng, Fractional quantum hall effect of hard-core bosons in topological flat bands, *Physical review letters* **107**, 146803 (2011).
- [47] N. Regnault and B. A. Bernevig, Fractional chern insulator, *Physical Review X* **1**, 021014 (2011).
- [48] T. Neupert, L. Santos, C. Chamon, and C. Mudry, Fractional quantum hall states at zero magnetic field, *Physical review letters* **106**, 236804 (2011).

- [49] D. Sheng, Z.-C. Gu, K. Sun, and L. Sheng, Fractional quantum hall effect in the absence of landau levels, *Nature communications* **2**, 389 (2011).
- [50] E. Tang, J.-W. Mei, and X.-G. Wen, High-temperature fractional quantum hall states, *Physical review letters* **106**, 236802 (2011).
- [51] K. Sun, Z. Gu, H. Katsura, and S. Das Sarma, Nearly flatbands with nontrivial topology, *Physical review letters* **106**, 236803 (2011).
- [52] J. Bloch, A. Cavalleri, V. Galitski, M. Hafezi, and A. Rubio, Strongly correlated electron–photon systems, *Nature* **606**, 41 (2022).
- [53] D. N. Basov, R. D. Averitt, D. Van Der Marel, M. Dressel, and K. Haule, Electrodynamics of correlated electron materials, *Reviews of Modern Physics* **83**, 471 (2011).
- [54] M. McGinley, M. Fava, and S. Parameswaran, Signatures of fractional statistics in nonlinear pump-probe spectroscopy, *Physical Review Letters* **132**, 066702 (2024).
- [55] G. Nambiar, A. Grankin, and M. Hafezi, Diagnosing electronic phases of matter using photonic correlation functions, *Physical Review X* **15**, 041020 (2025).
- [56] J. R. Vannucci, *Magneto-optical response of WSe_2 excitons in sub-Kelvin regime*, Ph.d. dissertation, University of Maryland, College Park, College Park, USA (2022).